RSC Advances

PAPER

View Article Online
View Journal | View Issue

Cite this: *RSC Adv.*, 2026, **16**, 9621

NaClO-oxidized cellulose nanofiber/chitosan composite films with improved water resistance and high mechanical strength

Madhurangika Panchabashini Horathal Pedige,[a] Rika Onishi,[a] Yoshiro Hatanaka,[b] Akihide Sugawara *[a] and Hiroshi Uyama *[a]

Cellulose nanofibers (CNFs) are increasingly recognized as sustainable alternatives to petroleum-derived plastics. However, their intrinsic hydrophilicity results in poor water resistance, which severely restricts applications in humid or aqueous environments. Therefore, improving water durability while maintaining mechanical performance remains a key challenge. In this study, we fabricated water-resistant composite films by combining oxidized CNFs (OCNFs), obtained *via* a simple sodium hypochlorite (NaClO) oxidation introducing carboxyl groups, with chitosan (CS). The OCNF/CS films exhibited markedly enhanced tensile strength (~50 MPa *vs.* ≤20 MPa for pristine OCNF) and retained their integrity in water for 24 h, with a swelling ratio of ~200% compared to ≥900% for OCNF alone. These improvements are attributed to strong ionic interactions between anionic carboxylate groups of OCNFs and cationic ammonium groups of CS, as well as hydrogen bonding within the polymer matrix. Furthermore, post-treatment with sodium hydroxide reinforced the network structure, raising tensile stress to ~80 MPa. The incorporation of glycerol as a plasticizer significantly improved wet-mechanical strength, with toughness increasing nearly threefold, as a result of suppressed hydration of polysaccharides. This fabrication method, with modifications, provided the ability to produce flexible, large-scale films. Overall, this work demonstrates that exploiting ionic interactions, hydrogen bonding, and simple post-treatments yields fully bio-based composite films with outstanding mechanical robustness, large scalability, and water resistance. These findings highlight the strong potential of OCNF/CS films as eco-friendly packaging materials for moisture-sensitive applications.

Received 8th January 2026
Accepted 27th January 2026

DOI: 10.1039/d6ra00188b

rsc.li/rsc-advances

Introduction

Biomass-based materials represent a promising solution to the environmental challenges posed by plastic pollution. As plastic consumption continues to rise globally, particularly in packaging, which accounts for approximately 32% of total use, plastic accumulates in large quantities on land and in the oceans. Alarmingly, most packaging waste is mismanaged, leading to significant environmental problems.[1] Moreover, the rapid pace of plastic production accelerates the depletion of petroleum resources.[2,3] The recycling of plastic is also costly due to its non-biodegradable nature. This highlights the urgent need to develop sustainable and effective alternatives across various applications.[4–6] Bio-based materials, derived from naturally renewable sources, are biodegradable and compostable, offering a distinct advantage in terms of mitigating carbon footprints and greenhouse gas emissions.[7] Polysaccharides are potential substitutes for petrochemical polymers in biomass-based material production because of their biodegradability and renewability. Additionally, materials made from polysaccharides demonstrate acceptable mechanical strength and gas barrier properties.[8]

Notably, cellulose is an ideal starting material for eco-friendly and sustainable plastic alternatives due to its renewable, biocompatible, and abundant nature. Cellulose nanofibers (CNFs) are especially attractive for their exceptional mechanical properties, derived from their crystalline structure and strong hydrogen bonds, making them suitable for application in a wide range of functional materials.[9–12] CNFs are produced through both physical and chemical methods. Although physical methods are advantageous in preserving the chemical structure of cellulose, they are often limited by high energy consumption and the need for sophisticated equipment. Chemical methods, in contrast, modify cellulose by introducing charged groups that promote fiber separation through electrostatic repulsion. A widely used approach is 2,2,6,6-tetramethyl-1-piperidinyloxy (TEMPO)-mediated oxidation, which

[a]*Department of Applied Chemistry, Graduate School of Engineering, The University of Osaka, 2-1 Yamadaoka, Suita, Japan. E-mail: a_sugawara@chem.eng.osaka-u.ac.jp; uyama@chem.eng.osaka-u.ac.jp; Tel: +81-6-6879-7365; +81-6-6879-7364*

[b]*Research Division of Biomaterials and Commodity Chemicals, Osaka Research Institute of Industrial Science and Technology Morinomiya Center, 1-6-50, Morinomiya, Joto-ku, Osaka 536-8553, Japan*

introduces carboxylic groups at the C6 position.[13] By contrast, sodium periodate cleaves the C2–C3 vicinal diol to give 2,3-dialdehyde cellulose. Sodium chlorite then oxidizes the aldehydes to carboxyl groups, increasing the carboxyl content but requiring two steps.[14,15] Recently, Isogai *et al.*[16] developed a one-pot oxidation method using aqueous $NaClO \cdot 5H_2O$. This technique also targets the C2–C3 glycol bond, yielding more carboxylic acids with lower chemical and energy requirements compared to traditional multi-step processes, making it a promising and efficient alternative.

Despite the advantage, the abundance of hydrophilic hydroxyl groups in the cellulose backbone renders cellulose-based materials highly sensitive to moisture, significantly reducing their wet mechanical strength and overall durability. This poses challenges in various applications.[17,18] Conventional approaches to enhancing the moisture resistance predominantly involve the incorporation of hydrophobic polymers or extensive chemical modifications of the cellulose backbone.[19–22] Although these methods can effectively improve wet stability, they often compromise the intrinsic role of cellulose by reducing its content and utilizing it primarily as a filler, which in turn lowers the overall biomass content. To enhance water resistance without sacrificing sustainability, bio-based complementary additives that are structurally and functionally compatible with cellulose are preferred.[23–26] In this context, chitosan (CS) has emerged as a promising cationic additive due to its natural origin, biodegradability, and strong affinity for cellulose.[27,28] CS is the deacetylated form of chitin, a naturally abundant polymer found in terrestrial arthropods, marine mollusks, and microorganisms.[29–32] In addition, CS is biodegradable, nontoxic, biocompatible, chemically stable, soluble in acidic aqueous media, and exhibits good film-forming properties. Through the formation of polyelectrolyte complexes with anionic CNFs, CS contributes to a marked improvement in the water stability of cellulose-based materials.[33–35]

In this study, we explore the fabrication of water-durable films through the electrostatic complexation of anionic CNFs, produced *via* one-pot NaClO oxidation (OCNFs), with cationic CS (Fig. 1). This oxidation approach not only introduces carboxylic groups but also facilitates efficient cellulose fibrillation under mild conditions. The combination of OCNFs and CS forms polyelectrolyte complexes through ionic interactions between the carboxylate of OCNFs and ammonium groups of CS. The formation of such complexes, along with strong inter- and intra-molecular hydrogen bonding among the polysaccharides, is anticipated to contribute to a dense, interconnected network structure with improved water resistance and mechanical robustness. Furthermore, additional processing strategies, such as mild base treatment and the incorporation of glycerol plasticizer, are employed to reduce the hydration of the materials, thereby enhancing water resistance while tailoring flexibility and mechanical performance. By leveraging fully bio-based and structurally compatible components *via* optimizing physical interactions, this approach presents a promising strategy for developing high-performance, biodegradable packaging materials with enhanced wet-state functionality.

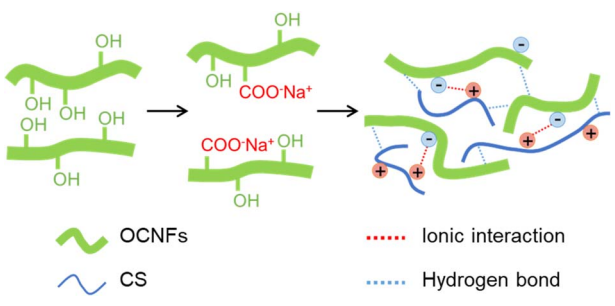

Fig. 1 Illustration of oxidation of cellulose using NaClO and the ionic interactions between OCNF and CS in the CNF/CS composite film.

Materials and methods

Materials

Microcrystalline cellulose (Avicel PH101) was purchased from Sigma-Aldrich Japan Co. (Tokyo, Japan). CS, acetic acid, NaOH, HCl, sodium chloride, and glycerol were purchased from Wako Chemicals (Osaka, Japan). $NaClO \cdot 5H_2O$ was purchased from Tokyo Chemical Industry (Tokyo, Japan). All solutions were prepared using deionized (DI) water as the solvent.

Preparation of oxidized cellulose nanofibers (OCNFs) dispersion

The oxidation was conducted according to the method of Isogai *et al.*,[16] with modifications. First, $NaClO \cdot 5H_2O$ (70 g) was dissolved in DI water to prepare an 18% (w/w) solution. The pH of the solution was adjusted to 10 by adding a concentrated HCl solution dropwise. Then, cellulose powder (4.9 g) was added to start the reaction. The reaction was performed at 30 °C with gentle stirring. An 8 mol per L NaOH solution was added to the reaction medium in intervals to maintain 10 pH. The reaction was performed for 60 min. Afterwards; the reaction sample was filtered through a 0.45 μm pore-sized PTFE membrane filter and washed with water to remove unreacted NaClO and byproducts. The solid residue was mixed with DI water and fibrillated using a laboratory blender (WARNING, Osaka Chem., Japan). The quantity of carboxylate groups was measured by conductometric titration according to the method of Isogai *et al.*[36] The freeze-dried samples were then characterized by Fourier transform infrared (FTIR) spectroscopy (Thermo Scientific Nicolet iS 5, USA). Scanning electron microscopy (SEM) (Hitachi SU3500, Japan) was used to observe the morphology of the samples. The freeze-dried samples were sputtered with gold-palladium using an MSP-1S magnetron sputter (Vacuum Device Inc., Japan) and then observed under high vacuum at an acceleration voltage of 15.0 kV. Transmission electron microscopy (TEM) was used to observe the aqueous suspension of OCNF fibers and the composite films using (TEM-2100IM JEOL Ltd. Japan), and ImageJ software was used to calculate lengths and diameters of the fibers.

Fabrication of OCNFs and chitosan (OCNF/CS) composite film and characterisation

CS was dissolved in 1.0% (w/w) acetic acid aqueous solution. OCNF dispersions of 2.0% (w/w) were mixed with 1.0% (w/w) CS solution in a predetermined ratio (denoted OCNF/CS-x, where x represents the weight ratio of CS solution to CNF dispersion). The mixtures were sufficiently stirred, and films were obtained by solution casting and drying overnight at 25 °C. X-ray Diffraction (XRD) analysis of the fabricated film was performed using a Multipurpose diffractometer (SmartLab, Rigaku Corporation, Japan). Then, thermogravimetric analysis (TGA) for the film was performed using the thermal analysis system (STA200RV, HITACHI, Japan).

Base treatment of composite film

The dried OCNF/CS-x films were immersed in 0.1 mol per L NaOH aqueous solution for 15 min, followed by repeated rinsing with DI water until the pH value of the washings became neutral. After draining the excess water, the films were left to dry by evaporation at 25 °C. The obtained films were denoted as b-OCNF/CS-x.

Fabrication of OCNF, CS, and glycerol (Gly)(OCNF/CS/Gly) film

The procedure for OCNF/CS-1 film preparation was modified with Gly treatment to produce OCNF/CS/Gly films. First, a 25% (w/w) glycerol solution was prepared using DI water. Then, the glycerol solution was added to the OCNF/CS-1 mixture in 10, 20, 30, 40, and 50% (w/w) OCNF. Films were obtained by solution casting, as previously described.

Water resistance characterization

The water resistance of OCNF/CS was tested by evaluating the film swelling ratio. After measuring the dry weight, the films were immersed in DI water. Wet weights were measured within predetermined time intervals until the swelling became constant. The calculation was performed using eqn (1), where SR is the swelling ratio, w_s is the weight of the swollen film, and w_d is the weight of the dry film.

$$SR = (w_s - w_d)/w_d \times 100 \quad (1)$$

Mechanical property characterization

The films were cut into strips with a length of 40 mm and a width of 5 mm. They were stretched using a universal testing machine (UTM, Shimadzu EZ graph, Japan) with a stretching speed of 5.0 mm min^{-1} at room temperature. The mechanical properties (maximum stress, strain at break, Young's modulus, and toughness) of the films were calculated using stress–strain curves. Three replicates were used for each measurement, and the average values were calculated. The wet strengths of the films were determined by immersing the films in DI water for 24 h. Measurements were performed similarly to dry films.

Results and discussion

Oxidation of cellulose

Oxidation of cellulose was conducted using highly concentrated NaClO. Following oxidation, the cellulose was fibrillated using a standard laboratory blender, without the need for specialized equipment. FT-IR spectroscopy was used to confirm the introduction of carboxylate groups into the cellulose. All characteristic peaks associated with the native cellulose spectrum were also observed in the oxidized cellulose spectrum. However, after oxidation, a strong peak at 1612 cm^{-1} appeared corresponding to the asymmetric carboxylate stretching vibration (Fig. 2a). The resulting cellulose fiber aqueous suspension was well-dispersed and exhibited long-term stability (Fig. 2c). A fine separation of fibres was also observed in SEM images (Fig. 2d). According to TEM images, the length of the nanofibers is approximately 127 $\pm$ 32 nm, the diameter of the nanofibers is around 4.2 $\pm$ 2.1 nm, with an aspect ratio of 31 $\pm$ 17 (Fig. 2e and S1). The CNFs' zeta potential value of −34.9 mV further confirms the successful production of negatively charged carboxylate groups by oxidation. Oxidation conditions were optimized by varying several parameters, including pH, NaClO concentration, and oxidation time (Table S1 and Fig. S2). The optimal conditions were selected based on the final yield, carboxylate content, and the dispersibility of the final product. Under these optimized conditions, the carboxylate content of the CNF dispersion reached 0.69 mmol g^{-1}, as determined by conductometric titration. This oxidation was predicted to be selective on the vicinal alcohols at the C2 and C3 positions, introducing two carboxylate groups[37] (Fig. 2b). The observed stability of the OCNFs suspension is attributed to electrostatic repulsion between the introduced carboxylate groups. The retention of the native cellulose special features, alongside the emergence of carboxylate peaks, confirms successful functionalization without compromising the cellulose backbone. The one-pot oxidation method enabled effective fibrillation of cellulose and offered an industrially and environmentally favourable approach. The process was demonstrated to operate at near-room temperature and atmospheric pressure, making it suitable for scalable and sustainable applications.

Fabrication and characterization of the OCNF/CS film

Composite films of OCNFs and CS were fabricated by a solution casting method. Films were evaluated for their morphology and the mechanical properties. TEM images of the film reveal nanometer-scale fibers aligned in a common direction, supporting the bundling of OCNF fibers within the film matrix (Fig. 3a–c). The XRD pattern of the OCNF/CS composite film exhibited a sharp diffraction peak corresponding to the (2 0 0) crystallographic plane of cellulose (Fig. S3b). Additionally, the TGA results showed that the composite film decomposed at around 300 °C, which was comparable to the thermal degradation behavior of the individual CS and OCNF samples (Fig. S4 and Table S2). In addition, the FTIR spectrum of the OCNF/CS composite exhibited characteristic absorption bands derived from both OCNFs and CS (Fig. S3a). In the dry state, OCNF films

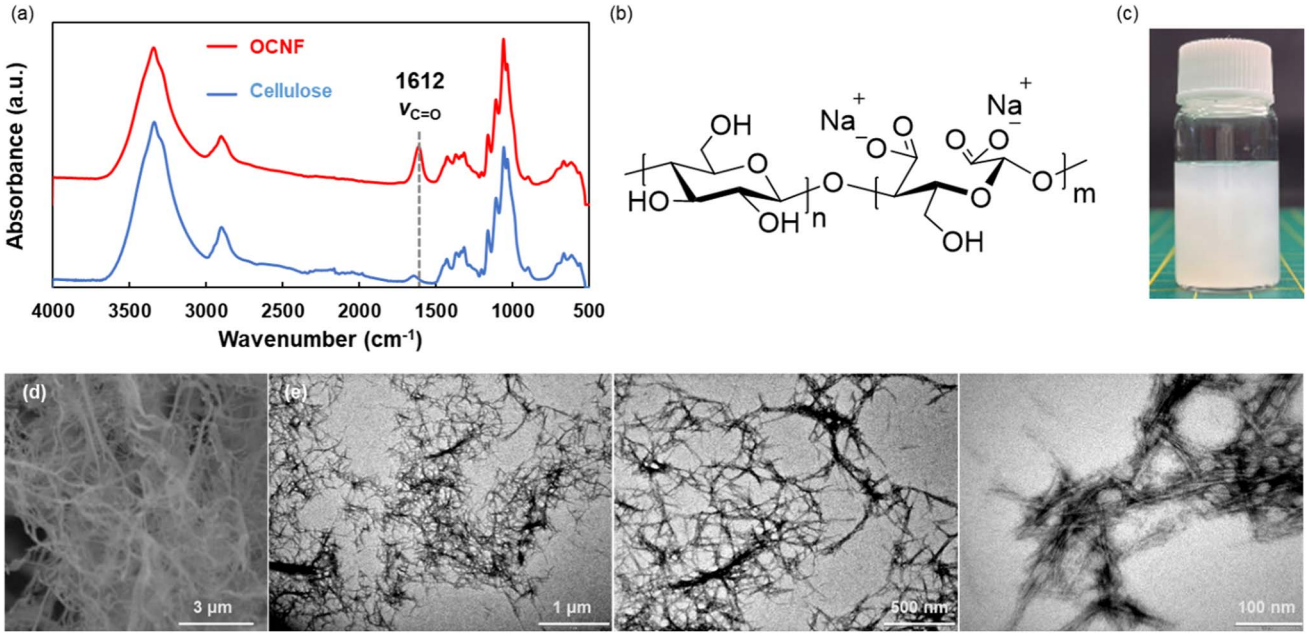

Fig. 2 (a) FT-IR spectra of cellulose and OCNFs. (b) Chemical structure of the OCNFs. (c) Photograph of OCNF aqueous dispersion. (d) SEM image of OCNFs. (e) TEM images of the OCNFs at different magnifications.

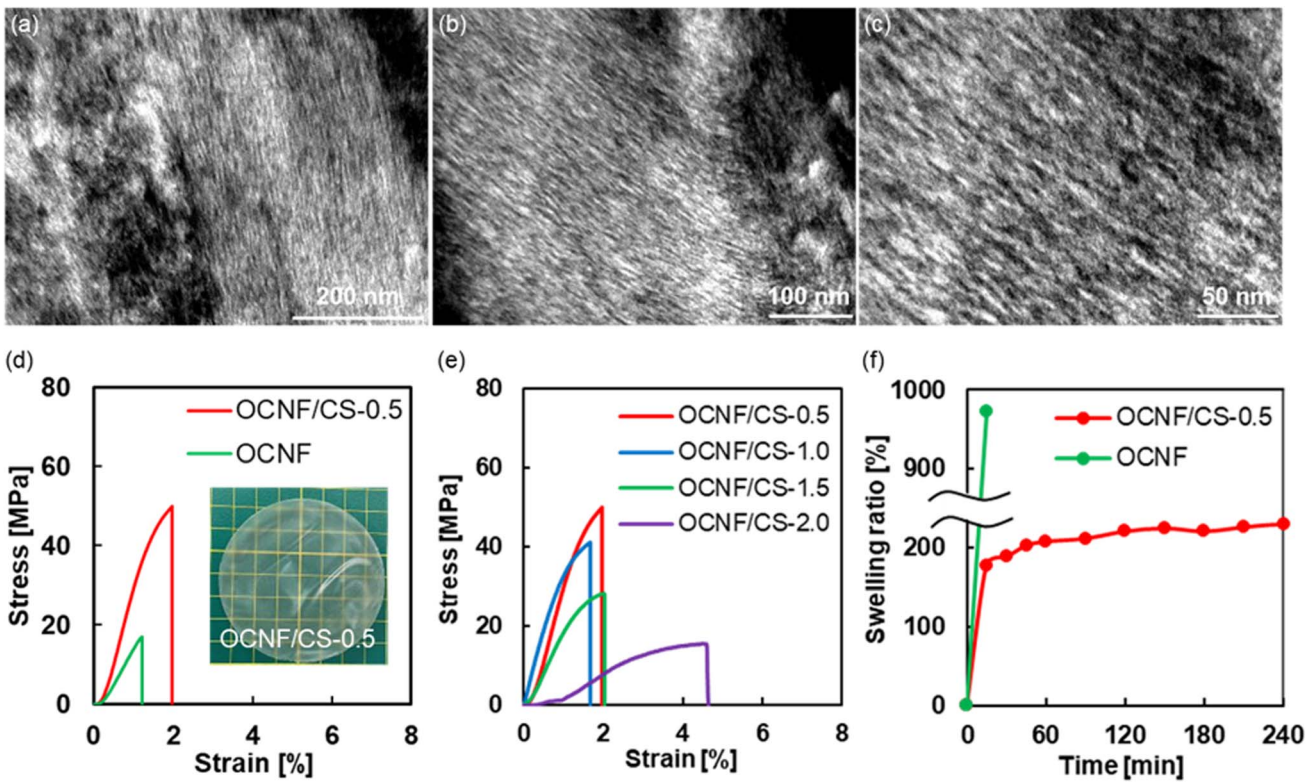

Fig. 3 (a–c) TEM images of OCNF/CS composite film at different magnifications. (d) Stress–strain curves of OCNFs and OCNFs/CS films in the dry state. (e) Stress–strain curves OCNF/CS films with different OCNF dispersion to CS solution weight ratios, in the dry state. (f) Swelling ratio of OCNF and OCNF/CS-0.5 films.

exhibited a maximum stress of ≤20 MPa, and the strain at break was ~1% (Fig. 3d). In contrast, OCNF/CS-1 films demonstrated a markedly enhanced tensile strength of ~50 MPa and a strain at break of ~2%, mainly due to the inherent brittleness of cellulose nanofibers. As the CS concentration increased, the films exhibited greater flexibility and strain (Fig. 3e). This

improvement is attributed to strong physical interactions such as hydrogen bonding and ionic interactions between the carboxylate groups of OCNFs and the ammonium groups of CS, which reduced brittleness and enhanced flexibility. Also, the mechanical strength of the present film was comparable to that of poly(lactic acid) (PLA) and poly(3-hydroxybutyrate-*co*-3-hydroxyvalerate) (PHBV) (Table S3). Furthermore, larger square-shaped films (22 × 22 cm) were successfully fabricated, demonstrating the scalability of the material (Fig. S5).

The water resistance of the films was determined by immersing dry samples in DI water. OCNF film showed a swelling ratio of ≥900% within just 15 min of immersion, ultimately disintegrating and losing its original shape (Fig. 3f). In contrast, the OCNF/CS-1 film displayed a significantly lower swelling ratio, of ~200%, and maintained its shape even after 24 h of immersion (Fig. S6a). This indicates that the strong interactions between OCNF and CS effectively suppressed swelling and significantly enhanced the water durability of OCNF/CS films.

Moreover, biodegradability of the dried OCNF/CS film was primarily assessed using a soil burial test conducted under natural forest soil conditions. A film specimen (2 cm × 2 cm) was buried under natural weather conditions for two weeks. The film gradually showed visible signs of degradation over time (Fig. S6b), confirming that the fabricated material is biodegradable and capable of self-decomposition, making it potentially suitable for sustainable packaging applications.

Fabrication and characterisation of the base-treated OCNF/CS (b-OCNF/CS) film

To improve the mechanical properties and water stability of OCNF/CS films, a base treatment was applied. In the base treatment, the OCNF/CS films were immersed in a diluted NaOH aqueous solution for a short time. The untreated OCNF/CS film in the dry state exhibited a maximum stress of 50 MPa and strain at break 2%, while those of b-OCNF/CS reached 80 MPa and 8% (Fig. 4a). Furthermore, the toughness of b-OCNF/CS was markedly enhanced following base treatment across all film compositions of OCNF and CS; among them, b-OCNF/CS-3 exhibited the highest toughness (Fig. 4b). The purpose of base treatment was to promote physical entanglements between OCNFs–CS and CS–CS. Upon short-duration base treatment, the CS hydration decreased due to the deprotonation of some ammonium groups in CS. This dehydration promoted the strong adsorption of CS chains to the OCNF surfaces *via* physical bonding, thereby strengthening the interface between the OCNFs and CS.[38] Additionally, the reduction in electrostatic repulsion between CS chains facilitated denser physical bonding, leading to the formation of an intertwined CS network. During the drying process, this network densified, enhancing the network strength.[39] Overall, the base treatment improved the mechanical properties of the b-OCNFs/CS composites by strengthening the physical entanglements between polymer chains.

The water durability of the films was evaluated by immersing the films in DI water after the base treatment. The swelling

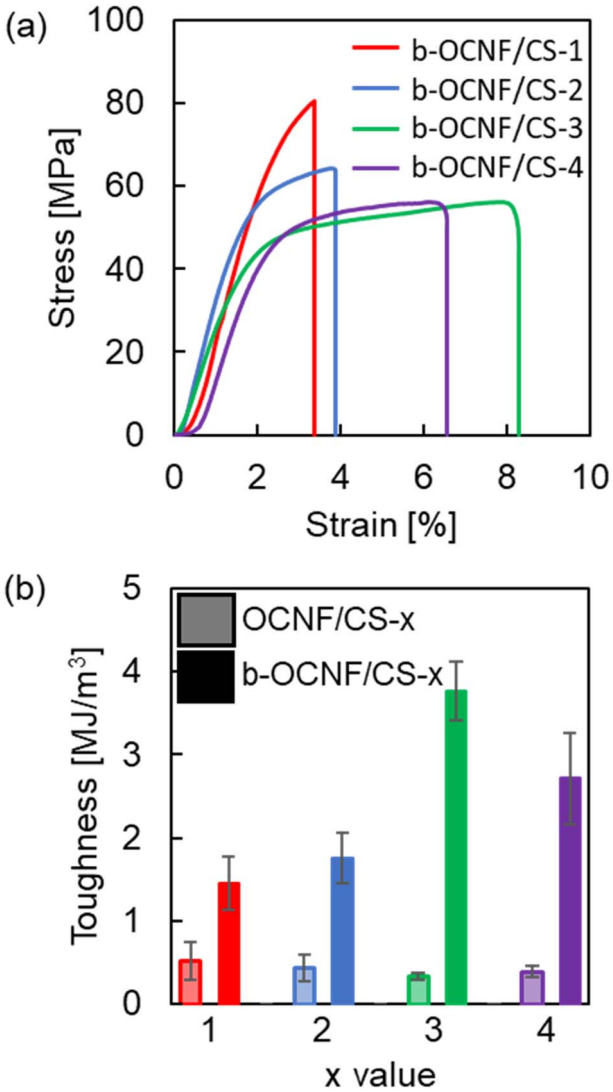

Fig. 4 (a) Stress–strain curves of b-OCNF/CS films in the dry state. (b) Toughness of pristine and b-OCNF/CS films with different amounts of CS in dry states.

behavior and the mechanical properties in the wet state were considered. A significant reduction in the swelling ratio was observed, decreasing from ~250% to below 100% (Fig. 5a). As the CS content increased, the swelling capacity markedly declined, with samples exhibiting maximum swelling of only ~30%, even after 24 h of immersion in water. Mechanical properties in the wet state were compared between OCNF/CS-1 and b-OCNF/CS-1. The maximum stress of b-OCNF/CS films showed a significant improvement, from below ~1 MPa to above 5 MPa (Fig. 5b). Additionally, the strain at break of b-OCNF/CS increased with increasing CS content in the base-treated films. b-OCNF/CS exhibited higher Young's modulus and toughness than OCNS/CS, with toughness increasing with increasing CS content (Fig. 5c). Fig. 5d demonstrates b-OCNF/CS films' ability to support a weight of 87 g (100 g in air) underwater for 24 h without failing. To further support the effect of base treatment on wet stability, the swelling behavior of

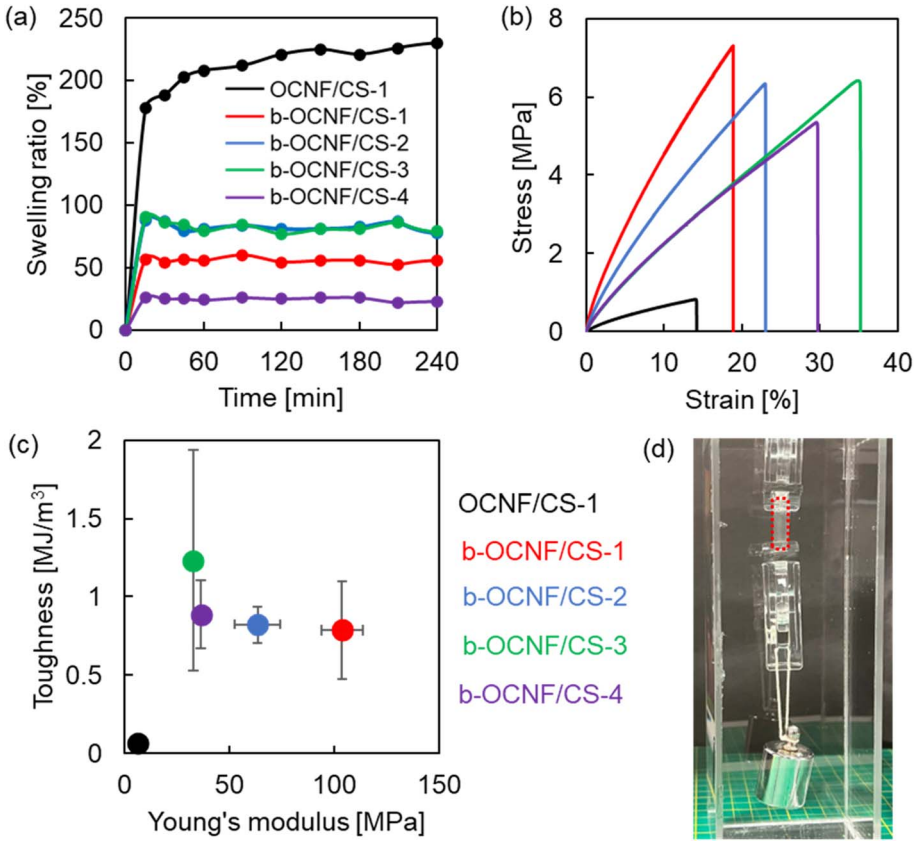

Fig. 5 (a) Swelling ratio, (b) stress–strain curves, and (c) toughness and Young's modulus graph of OCNF/CS-1 b-OCNF/CS films in wet states. (d) Photograph of around 87 g (100 g in air) weight supported by a b-OCNF/CS film in water.

the composite films was evaluated under different pH conditions (pH 2, 7, and 12). The base-treated films exhibited low swelling ratio at pH 7 and 12 (Fig. S11a). In contrast, significantly higher swelling was observed at pH 2, which can be attributed to the increased solubility and protonation of CS under acidic conditions. The wet mechanical properties exhibited the same trend as the swelling behavior, confirming the wet stability of the composites at neutral and basic conditions (Fig. S11b and c). The effect of base treatment on CS was further confirmed by increasing the OCNF content during treatment. This increase did not significantly improve the swelling ratio or mechanical properties (Fig. S7a). To further support this, the treatment was applied to CS-only films (denoted b-CS). While untreated CS films swelled and disintegrated rapidly upon immersion, b-CS films retained their shape even after 24 h in water. In both dry and wet states, b-CS showed significantly improved mechanical strength (Fig. S8) Notably, base treatment enhanced the water stability of the films, even in compositions with high CS content, effectively reducing swelling and preventing structural failure. This reduction is attributed to the dense physical interactions among the polymer chains, which enhance the interfacial interactions. Additionally, the strong network of the CS polymer chains can restrict the water uptake by limiting the formation of an aqueous layer within the composite matrix. Base treatment deprotonated the ammonium groups in CS, thereby reducing its interaction with water molecules. Furthermore, the formation of a highly intertwined network structure through interchain interactions among CS polymers contributed to the high strength of the composite films. These findings suggest that structural and morphological changes in CS, resulting from the deprotonation of ammonium groups due to base treatment, particularly its strong polymer network, were the primary contributors to the enhanced properties of b-OCNF/CS composites. Overall, the base treatment imparted OCNF/CS films with superior water resistance and improved mechanical performance under wet conditions.

Fabrication and characterization of the OCNF/CS/Gly film

To further evaluate the mechanical and water stability, glycerol was added to the composite films as a plasticizer in varying weight ratios to the OCNFs. The dried films were evaluated for mechanical strength. The strain at break of OCNF/CS/Gly films increased with higher glycerol concentration (Fig. 6a). Notably, when 10% (w/w) glycerol was added, the toughness increased to approximately three times that of OCNF/CS-1, while the Young's modulus remained nearly unchanged (Fig. 6b). To gain insight into the hydrogen-bonding behavior of the OCNF/CS/Gly films, IR spectroscopy was performed. (Fig. S10). A broad absorption band observed around 3300 cm^{-1} is mainly attributed to the O–H stretching vibrations of glycerol and polysaccharides. The

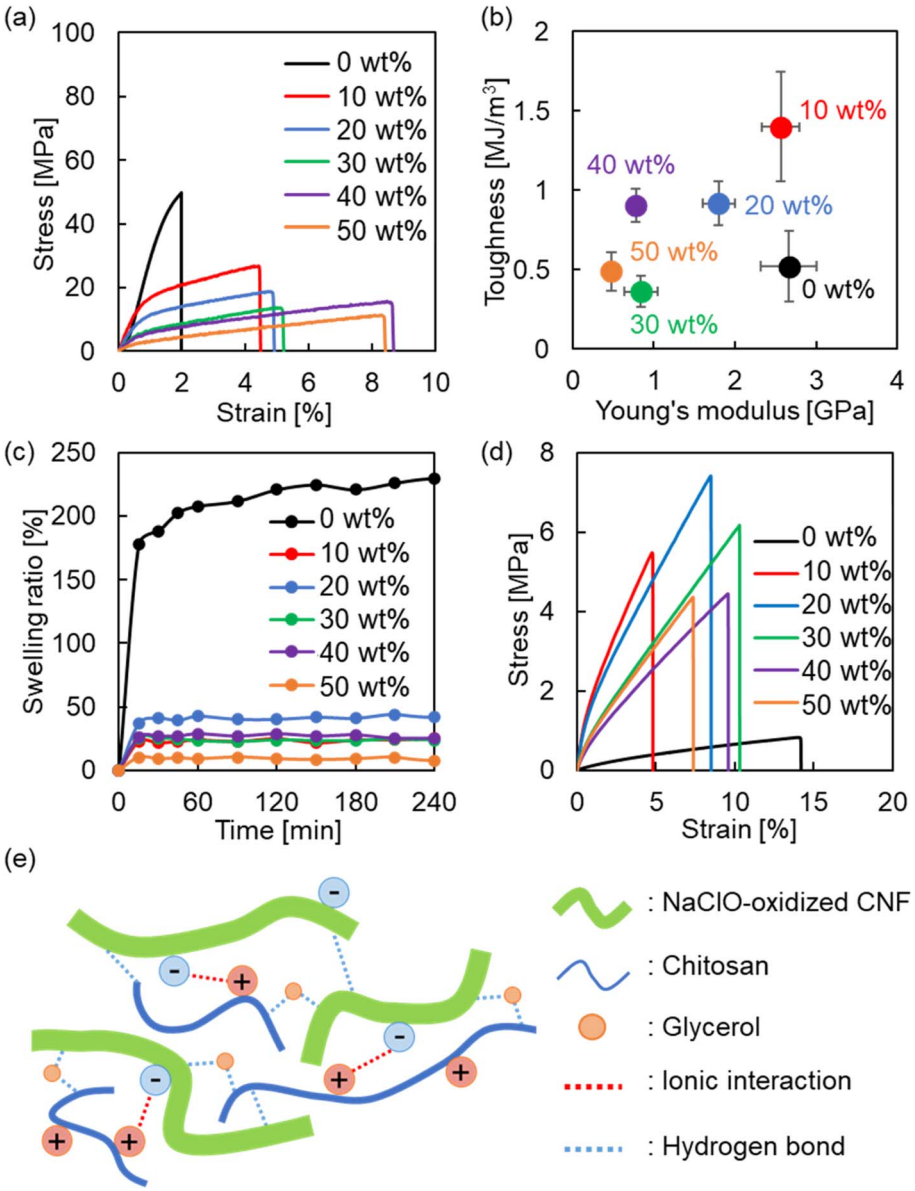

Fig. 6 (a) Stress–strain curves and (b) toughness against Young's modulus of OCNF/CS/Gly with varying glycerol contents in dry state. (c) Swelling ratio and (d) stress–strain curves of OCNF/CS/Gly with varying glycerol contents in wet state. (e) Illustration of interactions among OCNFs, CS, and glycerol in OCNF/CS/Gly.

films containing 10 and 20 wt% glycerol exhibited peak maxima near 3330 cm^{-1}, similar to the film without glycerol. In contrast, when the glycerol content was increased to 30–50 wt%, a shift toward higher wavenumbers was observed, and the peak maximum appeared at approximately 3340 cm^{-1}. This shift to higher wavenumbers indicates a weakening of the hydrogen-bonding network within the films due to the incorporation of excess glycerol. On the other hand, in the films containing 10 and 20 wt% glycerol, the results support the formation of hydrogen bonds between glycerol and the polysaccharides within the film matrix. This interpretation correlates well with the mechanical properties, as the films containing 10 and 20 wt% glycerol maintained relatively high Young's moduli, whereas a significant decrease in the modulus was observed for films containing 30 wt% or more glycerol (Fig. 6b). As a polyol, glycerol functions as a plasticizer by enhancing the flexibility of materials and reducing their brittleness. When incorporated into cellulose composites, the glycerol disrupts the strong interchain hydrogen bonding in cellulose chains, increasing chain mobility and enabling more flexible interactions among the chains (Fig. 6e). This modification softens the overall structure, making it more pliable and less rigid.[40,41] However, because excessive disruption of hydrogen bonds between the main components weakens the composite structure, the glycerol content should be optimised. Based on the results, a 10% glycerol content can be considered the optimal amount. Overall, the addition of glycerol can enhance mechanical strength by

acting as a plasticizer, and this effect can be tuned by adjusting the glycerol content.

The water resistance of the films was evaluated by immersing the films in DI water. The swelling behavior and the mechanical strength in wet states were evaluated. Regardless of the glycerol concentration, the swelling ratio decreased, and no significant differences were observed among the various glycerol concentrations (Fig. 6c). The swelling ratio of the samples with glycerol did not exceed 50%, even after 24 h of immersion in DI water (Table S4). Furthermore, the swelling behavior of the samples was evaluated under different pH conditions (pH 2, 7, and 12). Compared with the films without glycerol, the OCNFs/CS/Gly films exhibited improved stability across all pH conditions, as evidenced by reduced swelling (Fig. S11a). In the wet state, the maximum stress of OCNF/CS/Gly films increased significantly (Fig. 6d). Moreover, the addition of glycerol improved the toughness of the composite films. Notably, when 10% (w/w) glycerol was added, the Young's modulus reached 3.1 GPa (Fig. S9). Films gained this water durability because glycerol reduces the availability of free hydroxyl groups in cellulose composites, thereby limiting their capacity to absorb water. This is because glycerol has a strong affinity for the hydroxyl groups of polysaccharides, which allows it to effectively compete with water molecules hydration sites. As a result, the strong bonding between glycerol and hydroxyl groups reduced the composite's equilibrium moisture content.[42] Moreover, the OCNF/CS/Gly films exhibited stable wet mechanical strength at both acidic and basic conditions (Fig. S11d). These results demonstrate that incorporating glycerol into the composite film formulation not only enhanced mechanical properties but also significantly improved water stability.

Conclusions

An oxidized CNF dispersion in water with a sufficient carboxylate content was successfully prepared using NaClO, followed by a simple mechanical treatment. This was an eco-friendly method, requiring lower chemical and energy consumption compared to the other chemical methods, as mild conditions were sufficient to introduce a significant number of carboxylate groups. The oxidation resulted in a fine water suspension of CNFs functionalized by carboxylate groups, which was advantageous in composite synthesis. Water-resistant OCNF composite films were successfully prepared by utilizing possible interactions such as ionic interactions between the carboxylate groups in CNF and the ammonium groups in CS. The incorporation of CS into the network of OCNFs enhanced both the mechanical properties and water stability of the films due to these strong ionic interactions. Additionally, b-OCNF/CS obtained through base treatment of OCNF/CS exhibited excellent water resistance as well as high mechanical strength and toughness in the wet state. Moreover, OCNF/CS/Gly films prepared by adding glycerol as a plasticizer had a higher flexibility than OCNF/CS while maintaining excellent water resistance. These composite films, composed of biomass-derived materials and exhibiting excellent water resistance and mechanical properties, hold strong potential as eco-friendly materials for a wide range of applications.

Author contributions

The manuscript was written through the contributions of all authors. All authors have approved the final version of the manuscript. H. P. M. P.: investigation, writing – original draft, writing – review & editing. O. R. investigation, writing – original draft, Y. H. performing and the advising TEM analysis. A. S.: project administration, writing, review & editing, funding acquisition. H. U.: supervision, writing – review & editing, funding acquisition.

Conflicts of interest

The authors declare no competing financial interest.

Abbreviations

CNF	Cellulose nanofiber
OCNF	Oxidized cellulose nanofiber
CS	Chitosan
Gly	Glycerol
TEMPO	2,2,6,6-Tetramethyl-1-piperidinyloxy
NaClO	Sodium hypochlorite
DI	Deionized
FT-IR	Fourier transform infrared
UTM	Universal testing machine
XRD	X-ray diffraction
TGA	Thermogravimetric analysis
b-OCNF/CS	Base-treated OCNF/chitosan
b-CS	Base-treated chitosan

Data availability

The data supporting the findings of this study are included in the supplementary information (SI). Supplementary information: Tables S1–S4, which detail the optimisation of cellulose oxidation and additional characterisation of the composite materials, and Fig. S1–S11, which present cellulose fibre characterisation by TEM, as well as composite material characterisation using FTIR, TGA, XRD, tensile testing, and further analyses. See DOI: https://doi.org/10.1039/d6ra00188b.

Acknowledgements

This research was supported by JST, CREST, Japan (Grant Number JPMJCR24S5 and JPMJCR22L4)., and the Environment Research and Technology Development Fund JPMEERF21S11900, 3G-2501, and 3RA-2501 of the Environmental Restoration and Conservation Agency of Japan, JSPS KAKENHI Grants (no. 23K26717 and 24K17735). M. P. H. P. would like to thank the Ministry of Education, Culture, Sports, Science and Technology (MEXT) for scholarship support.

References

1 A. S. Pottinger, R. Geyer, N. Biyani, C. C. Martinez, N. Nathan, M. M. Morse, C. Liu, S. Hu, M. D. Bruyn, C. Boettiger, E. Baker and D. J. MacCauley, Pathways to reduce global plastic waste mismanagement and greenhouse gas emissions by 2050, *Science*, 2024, **386**, 1168–1173, DOI: 10.1126/science.adr3837.

2 E. N. Kalali, S. Lotfian, M. E. Shabestari, S. Khayatzadeh, C. Zhao and H. Y. Nezhad, A critical review of the current progress of plastic waste recycling technology in structural materials, *Curr. Opin. Green Sustainable Chem.*, 2023, **40**, 100763, DOI: 10.1016/j.cogsc.2023.100763.

3 Plastics give and plastics take, *Nat. Rev. Mater.*, 2022, **7**, 67, DOI: 10.1038/s41578-022-00419-y.

4 M. Morrison, R. Trevisan, P. Ranasinghe, G. B. Merrill, J. Santos, A. Homg, W. C. Edward, N. Jayasundara and J. A. Somarelli, A growing crisis for One Health: Impacts of plastic pollution across layers of biological function, *Front. Mar. Sci.*, 2022, **9**, 980705, DOI: 10.3389/fmars.2022.980705.

5 S. Huiting, R. J. Pugh and E. Forssberg, A Review of Plastics Waste Recycling and the Flotation of Plastics, *Resour. Conserv. Recycl.*, 1999, **25**, 85–109, DOI: 10.1016/S0921-3449(98)00017-2.

6 A. O. C. Iroegbu, S. S. Ray, V. Mbarane, J. C. Bordado and J. P. Sardinha, Plastic Pollution: A Perspective on Matters Arising: Challenges and Opportunities, *ACS Omega*, 2021, **6**, 19343–19355, DOI: 10.1021/acsomega.1c02760.

7 J. G. Rosenboom, R. Langer and G. Traverso, Bioplastics for a circular economy, *Nat. Rev. Mater.*, 2022, **7**, 117–137, DOI: 10.1038/s41578-021-00407-8.

8 C. Lim, S. Yusoff, C. G. Ng, P. E. Lim and Y. C. Ching, Bioplastic made from seaweed polysaccharides with green production methods, *J. Environ. Chem. Eng.*, 2021, **9**, 105895, DOI: 10.1016/j.jece.2021.105895.

9 J. Torifol and R. Moriana, Barrier packaging solutions from residual biomass: Synergetic properties of CNF and LCNF in films, *Ind. Crops Prod.*, 2022, **177**, 114493, DOI: 10.1016/j.indcrop.2021.114493.

10 D. Zhao, Y. Zhu, W. Cheng, W. Chen, Y. Wu and H. Yu, Cellulose-Based Flexible Functional Materials for Emerging Intelligent Electronics, *Adv. Mater.*, 2021, **33**, 2000619, DOI: 10.1002/adma.202000619.

11 S. Ji, B. Hyun, K. Kim, S. Y. Lee, S. H. Kim and J. Y. Kim, Photo-patternable and transparent films using cellulose nanofibers for stretchable origami electronics, *NPG Asia Mater.*, 2016, **8**, e299, DOI: 10.1038/am.2016.113.

12 X. Xu, J. Zhou, L. Jiang, G. Lubineau, T. Ng, B. S. Ooi, H. Y. Liao, C. Shen, L. Chen and J. Y. Zhu, Highly transparent, low-haze, hybrid cellulose nanopaper as electrodes for flexible electronics, *Nanoscale*, 2016, **8**, 12294–12306, DOI: 10.1039/C6NR02245F.

13 A. Isagai, T. Saito and H. Fukuzumi, TEMPO-oxidized cellulose nanofibers, *Nanoscale*, 2011, **3**, 71–85, DOI: 10.1039/C0NR00583E.

14 H. Liimatainen, M. Visanko, J. A. Sirviö, O. E. M. Hormi and J. Niinimaki, Enhancement of the Nanofibrillation of Wood Cellulose through Sequential Periodate–Chlorite Oxidation, *Biomacromolecules*, 2012, **13**, 1592–1597, DOI: 10.1021/bm300319m.

15 A. Kramar, A. Ivanovska and M. Kostic, Regenerated Cellulose Fiber Functionalization by Two-step Oxidation Using Sodium Periodate and Sodium Chlorite - Impact on the Structure and Sorption Properties, *Fibers Polym.*, 2021, **22**, 2177–2186, DOI: 10.1007/s12221-021-0996-8.

16 S. Matsuki, H. Kayano, J. Takada, H. Kono, S. Fujisawa, T. Saito and A. Isogai, Nanocellulose Production via One-Pot Formation of C2 and C3 Carboxylate Groups Using Highly Concentrated NaClO Aqueous Solution, *ACS Sustainable Chem. Eng.*, 2020, **8**, 17800–17806, DOI: 10.1021/acssuschemeng.0c06515.

17 S. Nigam, A. K. Das, F. Matkawala and M. K. Patidar, An insight overview of bioplastics produced from cellulose extracted from plant material, its applications and degradation, *Environ. Sustain*, 2022, **5**, 423–441, DOI: 10.1007/s42398-022-00248-3.

18 K. Lee, Y. Jeon, D. Kim, G. Kwon, U. J. Kim, C. Hong, J. W. Choung and J. You, Double-crosslinked cellulose nanofiber based bioplastic films for practical applications, *Carbohydr. Polym.*, 2021, **260**, 117817, DOI: 10.1016/j.carbpol.2021.117817.

19 Y. Liu, Y. Chen and H. Qi, Recyclable cellulose nanofibers reinforced poly (vinyl alcohol) films with high mechanical strength and water resistance, *Carbohydr. Polym.*, 2022, **293**, 119729, DOI: 10.1016/j.carbpol.2022.119729.

20 A. Xu, Y. Wang, J. Gao and J. Wang, Facile fabrication of a homogeneous cellulose/polylactic acid composite film with improved biocompatibility, biodegradability and mechanical properties, *Green Chem.*, 2019, **21**(16), 4449–4456, DOI: 10.1039/C9GC01918A.

21 P. Kotcharat, P. Chuysinuan, T. Thanyacharoen, S. Techasakul and S. Ummartyotin, Development of bacterial cellulose and polycaprolactone (PCL) based composite for medical material, *Sustain. Chem. Pharm.*, 2021, **20**, 100404, DOI: 10.1016/j.scp.2021.100404.

22 T. Tamiya, R. Soni, Y. I. Hsu and H. Uyama, Highly Water-Tolerant TEMPO-Oxidized Cellulose Nanofiber Films Using a Maleic Anhydride/Wax Copolymer, *ACS Appl. Polym. Mater.*, 2021, **3**(9), 4625–4633, DOI: 10.1021/acsapm.1c00573.

23 S. S. Shazleen, T. A. T. Yasim-Anuar, N. A. Ibrahim, M. A. Hassan and H. Ariffin, Functionality of cellulose nanofiber as bio-based nucleating agent and nano-reinforcement material to enhance crystallization and mechanical properties of polylactic acid nanocomposite, *Polymers*, 2021, **13**, 389, DOI: 10.3390/polym13030389.

24 J. G. Jeon, H. C. Kim, R. R. Palem, J. Kim and J. K. Kang, Cross-linking of cellulose nanofiber films with glutaraldehyde for improved mechanical properties, *Mater. Lett.*, 2019, **250**, 99–102, DOI: 10.1016/j.matlet.2019.05.002.

25 B. Guo, W. Chen and L. Yan, Preparation of flexible, highly transparent, cross-linked cellulose thin film with high

mechanical strength and low coefficient of thermal expansion, *ACS Sustain. Chem. Eng.*, 2013, **1**, 1474–1479, DOI: 10.1021/sc400252e.

26 R. Soni, T. A. Asoh and H. Uyama, Cellulose nanofiber reinforced starch membrane with high mechanical strength and durability in water, *Carbohydr. Polym.*, 2020, **238**, 116203, DOI: 10.1016/j.carbpol.2020.116203.

27 R. Soni, Y. I. Hsu, T. A. Asoh and H. Uyama, Cellulose nanofiber reinforced starch film with rapid disintegration in marine environments, *J. Appl. Polym. Sci.*, 2022, **139**, 52776, DOI: 10.1002/app.52776.

28 Y. Jia, Y. I. Hsu and H. Uyama, A starch-based, crosslinked blend film with seawater-specific dissolution characteristics, *Carbohydr. Polym.*, 2023, **299**, 120181, DOI: 10.1016/j.carbpol.2022.120181.

29 E. Hajili, A. Sugawara, T. A. Asoh and H. Uyama, Fabrication of 3D Hierarchically Porous Chitosan Monoliths by Thermally Induced Phase Separation of Chemically Modified Chitin, *ACS Sustain. Chem. Eng.*, 2023, **11**, 5473–5484, DOI: 10.1021/acssuschemeng.2c06953.

30 M. P. Horathal Pedige, T. A. Asoh, Y. I. Hsu and H. Uyama, Stimuli-responsive composite hydrogels with three-dimensional stability prepared using oxidized cellulose nanofibers and chitosan, *Carbohydr. Polym.*, 2022, **278**, 118907, DOI: 10.1016/j.carbpol.2021.118907.

31 M. P. Horathal Pedige, A. Sugawara and H. Uyama, Multifunctional Chitosan Nanofiber-Based Sponge Materials Using Freeze−Thaw and Post-Cross-Linking Method, *ACS Omega*, 2024, **9**, 36464–36474, DOI: 10.1021/acsomega.4c04317.

32 P. M. P. Horathal, A. Sugawara and H. Uyama, Clusterization-triggered emission of polysaccharide-based microclusters induced by the co-assembly of chitosan nanofibers and dialdehyde carboxymethyl cellulose, *Bull. Chem. Soc. Jpn.*, 2024, **97**, 065, DOI: 10.1093/bulcsj/uoae065.

33 J. Fu, F. Yang and Z. Guo, The chitosan hydrogels: from structure to function, *New J. Chem.*, 2018, **42**, 17162–17180, DOI: 10.1039/C8NJ03482F.

34 D. I. Sánchez-Machado, J. López-Cervantes, M. A. Correa-Murrieta, R. G. Sánchez-Duarte, P. Cruz-Flores and G. S. la Mora-López, Chitosan, in *Nonvitamin and Nonmineral Nutritional Supplements*, ed. M. N. Sayed and S. S. Ana, Elsevier, CA, 2018, p. 485, DOI: 10.1016/B978-0-12-812491-8.00064-3.

35 S. C. M. Fernandes, C. S. R. Freire, A. J. D. Silvestre, C. P. Neto and A. Gandini, Novel materials based on chitosan and cellulose, *Polym. Int.*, 2011, **60**, 875–882, DOI: 10.1002/pi.3024.

36 T. Saito and A. Isogai, TEMPO-Mediated Oxidation of Native Cellulose. The Effect of Oxidation Conditions on Chemical and Crystal Structures of the Water-Insoluble Fractions, *Biomacromolecules*, 2004, **5**, 1983–1989, DOI: 10.1021/bm0497769.

37 M. Kirihara, R. Osugi, K. Saito, K. Adachi, K. Yamazaki, R. Matsushima and Y. Kimura, Sodium Hypochlorite Pentahydrate as a Reagent for the Cleavage of trans-Cyclic Glycols, *J. Org. Chem.*, 2019, **84**, 8330–8336, DOI: 10.1021/acs.joc.9b01132.

38 M. S. Toivonen, S. Kurki-Suonio, F. H. Schacher, S. Hietalala, O. J. Rojas and O. Ikkala, Water-Resistant, Transparent Hybrid Nanopaper by Physical Cross-Linking with Chitosan, *Biomacromolecules*, 2015, **16**, 1062–1071, DOI: 10.1021/acs.biomac.5b00145.

39 S. Li, H. Wang, Z. Wan, Y. Guo, C. Chen, D. Li, M. Zhu and Y. Chen, Strong, Water-Resistant, and Ionic Conductive All-Chitosan Film with a Self-Locking Structure, *ACS Appl. Mater. Interfaces*, 2022, **14**, 23797–23807, DOI: 10.1021/acsami.2c01118.

40 J. Tarique, S. M. Sapuan and A. Khalina, Effect of glycerol plasticizer loading on the physical, mechanical, thermal, and barrier properties of arrowroot (Maranta arundinacea) starch biopolymers, *Sci. Rep.*, 2021, **11**, 13900, DOI: 10.1038/s41598-021-93094-y.

41 J. J. Benitez, P. Florido-Moreno, J. Porras-vàrzquez, G. Tedeschi, A. Athanassiou, J. A. Heredia-Guerrero and S. Guzman-Puyol, Transparent, plasticized cellulose-glycerol bioplastics for food packaging applications, *Int. J. Biol. Macromol.*, 2024, **273**, 132956, DOI: 10.1016/j.ijbiomac.2024.132956.

42 M. Vàzquez, G. Velazquez and P. Cazòn, UV-Shielding films of bacterial cellulose with glycerol and chitosan. Part 2: Structure, water vapor permeability, spectral and thermal properties, *J. Food.*, 2021, **19**, 115–126, DOI: 10.1080/19476337.2020.1870565.